Constitutive model and numerical simulation of HSLA steel during isothermal compression

Constitutive model and numerical simulation of HSLA steel during isothermal compression

Ning Li [a,b], Yao Huang [a,b], Hui Zhang [a,b], Renheng Han [a,b], Chengzhi Zhao [a,b,*], and Hexin Zhang [a,b,*]

[a] College of Materials Science and Chemical Engineering, Harbin Engineering University, Harbin 150001, China
[b] Key Laboratory of Superlight Materials and Surface Technology, Ministry of Education

E-mail: zhaochengzhi@hrbeu.edu.cn, zhanghx@hrbeu.edu.cn

Abstract. The true stress-strain curve of HSLA steel was obtained though a MMS-200 experiment machine. The flow behavior of HSLA steel during isothermal compression at different deformation conditions was investigated. The result indicated the flow stress increases as the strain rate increases or the deformation temperature decreases, and the flow curves show obvious dynamic softening characteristics at low strain rate or high temperature. The peak stress constitutive equation was established and the activation energy be calculated as 437955 J/mol. The effective strain and flow stress during isothermal compression were studied by finite element method. The simulation results show that the effective strain distribution at different regions is inhomogeneous. The flow stresses obtained by FEM are consistent with the corresponding test results.

1. Introduction

HSLA (high strength low alloy) steel has interested great attention from researchers owning to its excellent corrosion resistance and mechanical properties, and is used as structural components widely in automobiles, bridges, ships, pipelines, pressure vessels, and containers in recent years [1, 2]. Steel with low carbon content and trace addition of strong carbides, such as V, Nb, and Ti, is called microalloyed steel [3, 4]. The grain of microalloyed steel can be significantly improved by TMCP (thermo mechanical control process) technology. HSLA steels' mechanical properties can be enhanced using combining microalloying with TMCP technology [5, 6]. It thus is very significant to study HSLA steel's thermal deformation behavior for improving mechanical properties. In general, most researchers used a constitutive model based on the peak stress or constitutive model compensated with strain to study materials' thermal deformation behavior. The constitutive model that is based on peak stress can describe peak stress' fluctuation only with temperatures and strain rates, and neglect strain's effect on stress. Although constitutive equations compensated with strain can be used to study the relationship among deformation temperatures, flow stress, strains and strain rates, the process of establishing the equation is too complicated and the calculation results of flow stress at a large strain rate are not very accurate. With computer technology's development, the numerical simulation has become an effective method to predict the thermal deformation behavior during isothermal compression [7, 8]. However, it is rarely reported that the flow behavior of HSLA steel during hot compression is studied by numerical simulation.

In this paper, HSLA steel's true stress-strain curves were obtained by a MMS-200 experiment machine. The flow behavior of HSLA steel during isothermal compression at different deformation conditions was investigated. The material constants were calculated and the constitutive model was established. The numerical simulation was used to predict the effective strain distribution and flow stress curves of HSLA steel during the isothermal compression process.

2. Experimental procedures

The investigated steel is HSLA steel, the composition (wt%) of this steel used was as follows: 0.013 C, 0.147 Si, 0.203 Cr, 0.534 Ni, 0.392 Cu, 0.135 Mo, 0.041 Nb, 1.17 Mn, and balance Fe. The size of the cylindrical specimen is $\Phi 8 * 15\ \mathrm{mm}$, and the specimens were cut by wire cut machine. The hot compression tests were performed by a MMS-200 test machine at temperatures of 900, 1000 and 1100 ºC, and strain rates of 0.01-1 s^{-1}. Fig. 1 is a schematic diagram for isothermal compression. Specimens were heated to 1250 ºC at 20 ºC/s and holding for 180 s to obtain a uniform austenite structure. Then the temperature was reduced to the isothermal compression temperature at 10 ºC/s and the temperature gradient was eliminated by holding for 20 s. When the true strain is compressed to 0.7, all specimens are quenched immediately. The deformed specimen was cut along the compression axis. After grinding and polishing, the axis section was etched in ethanol solution containing 5% nitric acid.

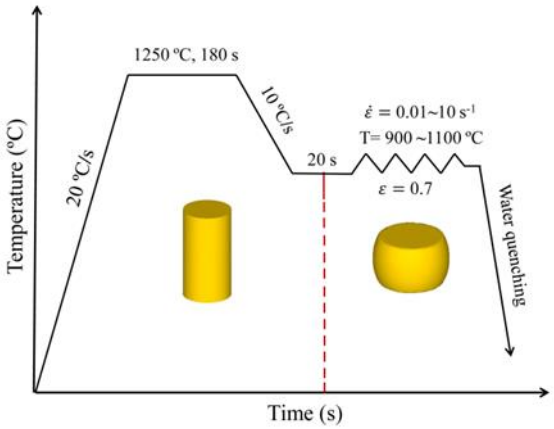

Fig. 1. The schematic diagram for hot compression test.

3. Results and Discussions

3.1. *Hot deformation behaviour*

The flow curves of the steel at varying strain rates and temperatures are presented in Fig. 2. It is observable that deformation temperatures and strain rates have important effects on flow stress. The flow stress increases as the strain rate increases or the deformation temperature decreases. At a definite strain rate, the flow stress increases with decreasing temperature. Dynamic recovery and DRX were performed more fully at a higher temperature, resulting in more obvious dynamic softening effect. Under a given temperature, with increasing strain rate, the flow stress was reduced. As demonstrated in Fig. 2 (d), at higher strain rates, dynamic recovery and dynamic recrystallization have no enough time to fully perform due to short deformation time. Therefore, compared to low strain rate, the dynamic softening effect is not obvious at the high strain rates.

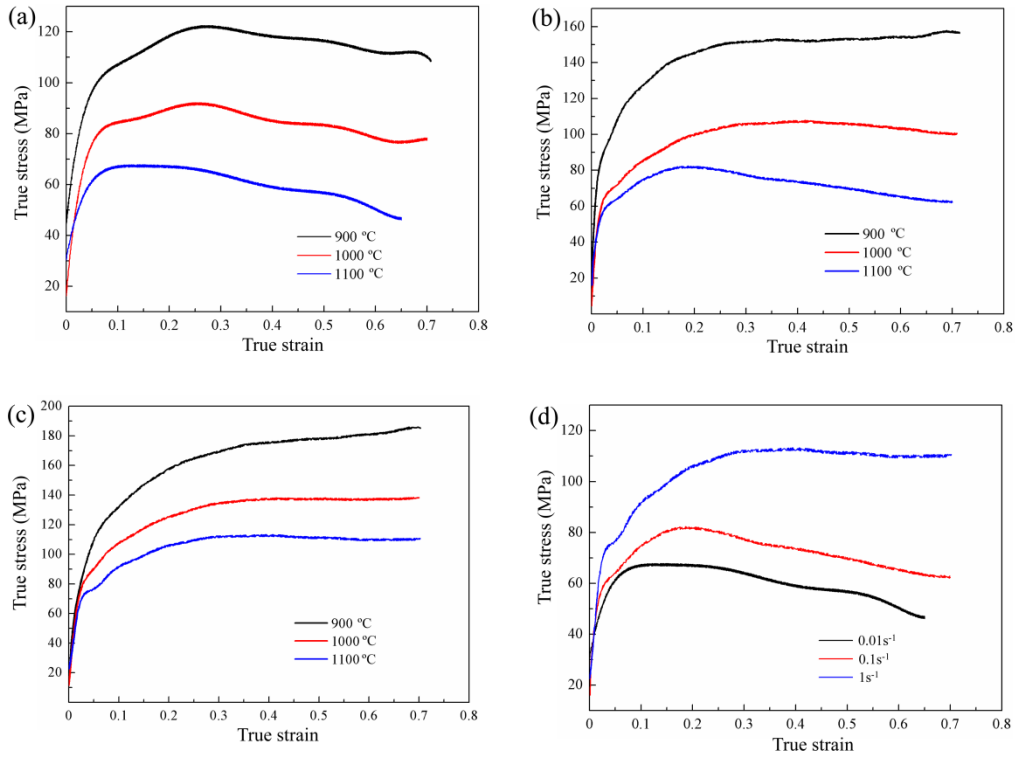

Fig. 2. The flow curves of HSLA steel at varying strain rates and temperatures: (a) 0.01s^{-1}, (b) 0.1 s^{-1}, (c) 1 s^{-1}, (d) 1100 ℃.

3.2. Constitutive equation

The flow stress is primarily influenced by the temperature, strain and strain rate, and the temperature and strain rate play a major role. The relationship between deformation temperature, flow stress and strain rate can be presented by the following kinetic equation.

$$Z = \dot{\varepsilon}\exp(Q/RT) \quad (1)$$

$$\dot{\varepsilon}\exp(Q/RT) = A_1\sigma_P{}^{n_1} \quad (when\ \alpha\sigma < 0.8) \quad (2)$$

$$\dot{\varepsilon}\exp(Q/RT) = A_2\exp(\beta\sigma_P) \quad (when\ \alpha\sigma > 1.2) \quad (3)$$

$$\dot{\varepsilon}\exp(Q/RT) = A[\sinh(\alpha\sigma_P)]^n \quad (for\ all\ \sigma) \quad (4)$$

In which, Z is the Z parameter, T is the hot deformation temperature (K), $\dot{\varepsilon}$ is the strain rate (s^{-1}), σ_P is the peak stress (MPa), Q is apparent activation energy ($J\cdot mol^{-1}$), R is the ideal gas constant (8.314 $J\cdot mol^{-1}\cdot K^{-1}$), n_1, β, A_1, A_2, A, and n are the material constants, where $\alpha = \beta/n_1$.

Taking the logarithm of the two sides of the Eqs. (2) and (3), and Eqs. (2) and (3) can be rewritten to Eqs. (5) and (6), respectively.

$$\ln\dot{\varepsilon} = n_1\ln\sigma_p + \ln A_1 - Q/RT \quad (5)$$

$$\ln\dot{\varepsilon} = \beta\sigma_p + \ln A_2 - Q/RT \quad (6)$$

The linear relation of $\ln\dot{\varepsilon} - \ln\sigma_P$ and $\ln\dot{\varepsilon} - \sigma_P$ at different strain rates are fitted, the fitting results are shown in Fig. 3a and 3b. The average slopes are used to calculate n_1 and β, which are 10.680 and

0.0927. According to $\alpha = \beta/n_1 = 0.00868$, the value of α can be calculated. When the deformation temperature is constant, Eq. (7) can be obtained by partial differential of Eq. (4).

$$n = \left[\frac{\partial \ln \dot{\varepsilon}}{\partial \ln[\sinh(\alpha\sigma_p)]}\right]_T \tag{7}$$

Similarly, at a given strain rate, Eq. (8) can be obtained by partial differential of Eq. (4).

$$Q = nR\left[\frac{\partial \ln[\sinh(\alpha\sigma_p)]}{\partial(1/T)}\right]_{\dot{\varepsilon}} \tag{8}$$

$$S = \left[\frac{\partial \ln[\sinh(\alpha\sigma_p)]}{\partial(1/T)}\right]_{\dot{\varepsilon}} \tag{9}$$

The values of n and S are obtained through the linear fitting slopes of Fig. 3c and 3d. The average values of n and S are 7.758 and 6047, respectively. Accordingly $Q = nRS$, the value of activation energy is calculated as 437955 J· mol^{-1}. By combining Eq. (4) and Eq. (1), Eq. (10) can be obtained. Taking the logarithm of the two sides of Eq. (10), and Eq. (10) is rewritten to Eq. (11).

$$Z = A[\sinh(\alpha\sigma_P)]^n \tag{10}$$

$$\ln Z = \ln A + n\ln[\sinh(\alpha\sigma_p)] \tag{11}$$

Fig. 4 shows a good linear relationship between $\ln Z$ and $\ln[\sinh(\alpha\sigma_P)]$. $\ln A$ is the intercept of the fitted curve, and $\ln A$ is calculated as 37.98 by linear fitting. The calculated results of material constants and Q are given in Table 1. Therefore, the constitutive equations of the steel based on peak stress can be obtained as following:

$$\dot{\varepsilon} = 3.12 \times 10^6[\sinh(0.00868\sigma_p)]^{7.758}\exp\left(-\frac{437955}{RT}\right) \tag{12}$$

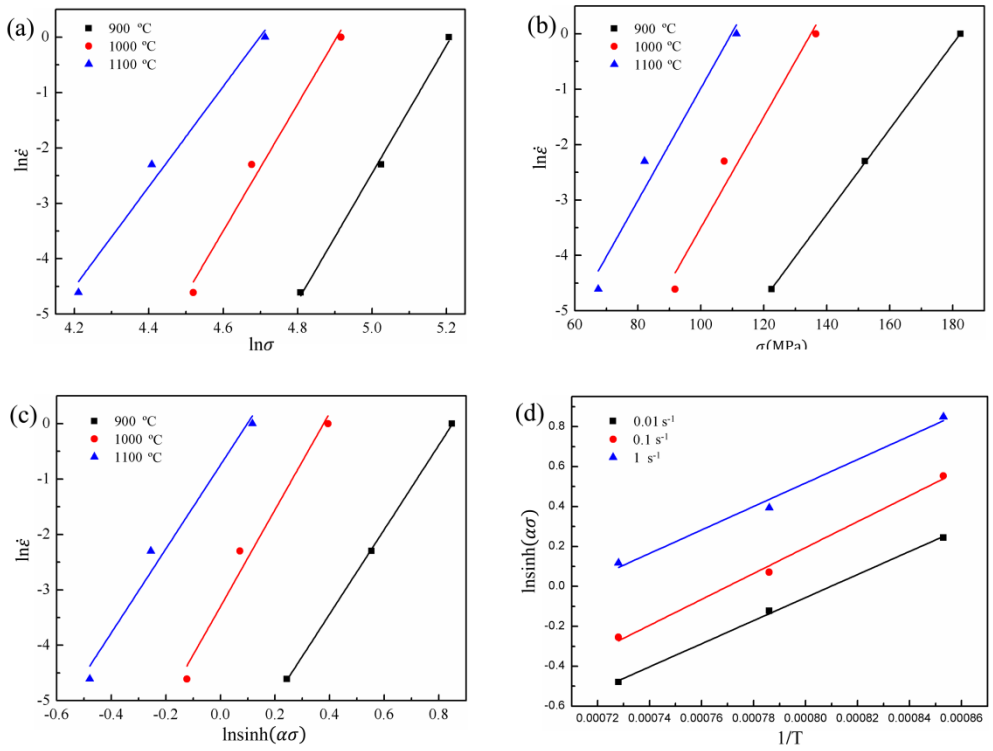

Fig. 3. Material constants solution for HSLA steel: (a) $\ln\dot{\varepsilon} - \ln\sigma$, (b) $\ln\dot{\varepsilon} - \sigma$,(c) $\ln\dot{\varepsilon} - \ln[\sinh(\alpha\sigma_p)]$, (d) $\ln[\sinh(\alpha\sigma_p)] - 1/T$.

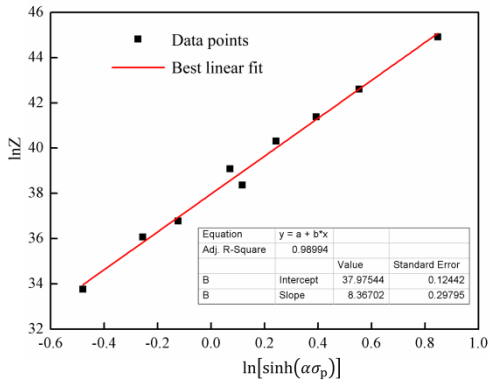

Fig. 4. Linear relationship between lnZ and $\ln[\sinh(\alpha\sigma_p)]$.

Table 1 Material constants for HSLA steel.

Parameter	n_1	β	α (Mpa^{-1})	n	Q ($J\cdot mol^{-1}$)	lnA
Value	10.680	0.0927	0.00868	7.758	437955	37.98

3.3. FEM simulation

Isothermal compression process for HSLA steel was simulated by using FEM (finite element method) under different deformation conditions. The flow stress data at varying deformation condition was obtained by isothermal compression test. The geometric model for FEM simulation is shown in Fig. 5.

The workpiece and dies were set as plastic type and rigid type, respectively. The friction type between workpiece and dies was set to shear type, the coefficient of friction is set to 0.6 [9]. The physical parameters for finite element analysis were calculated by Jmatpro software, and the calculated results are shown in Fig. 6. The commercial software package Deform-3D is used to simulate isothermal compression.

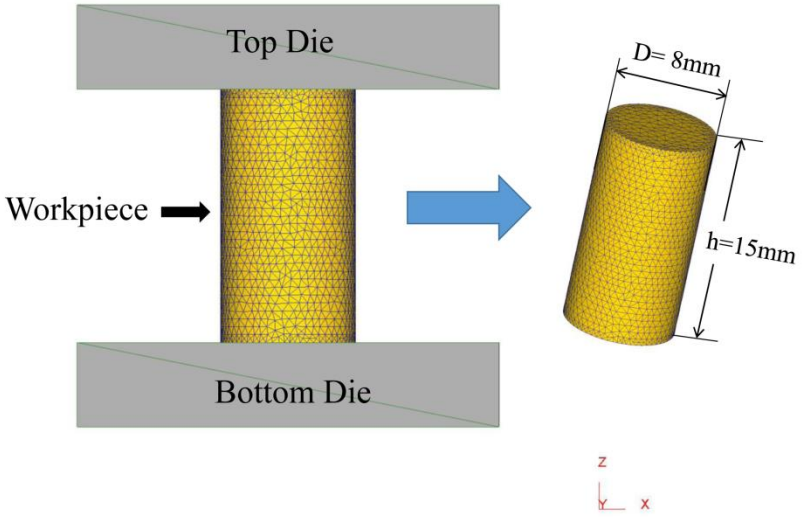

Fig. 5. FEM model of isothermal compression process.

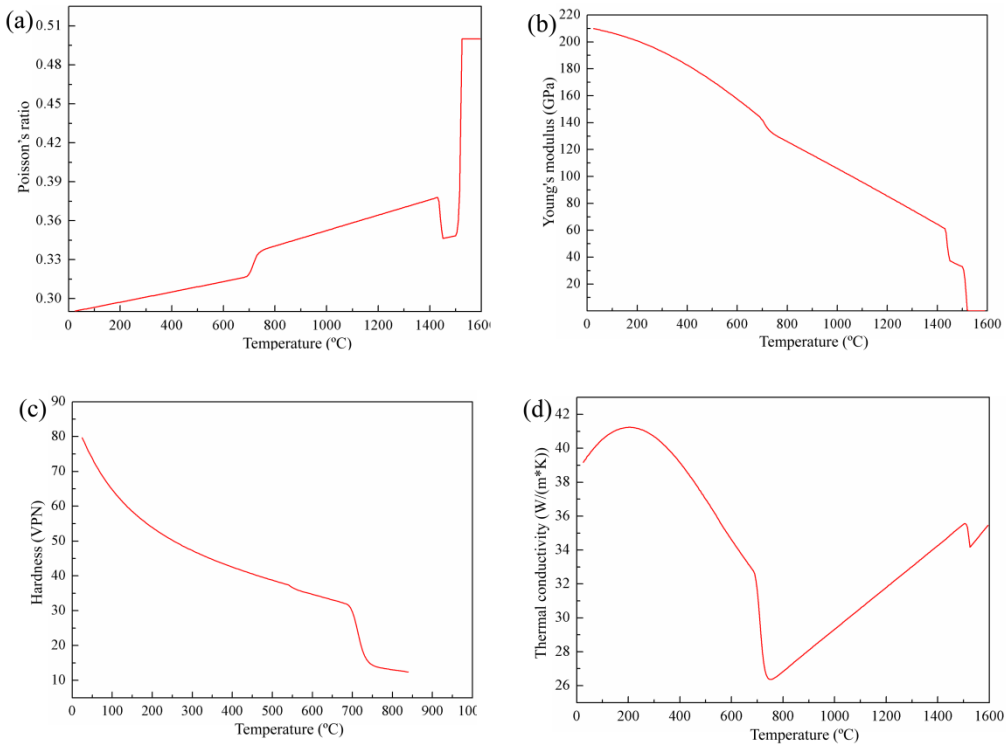

Fig. 6. Relationship between thermo-physical parameters and temperature of HSLA steel.

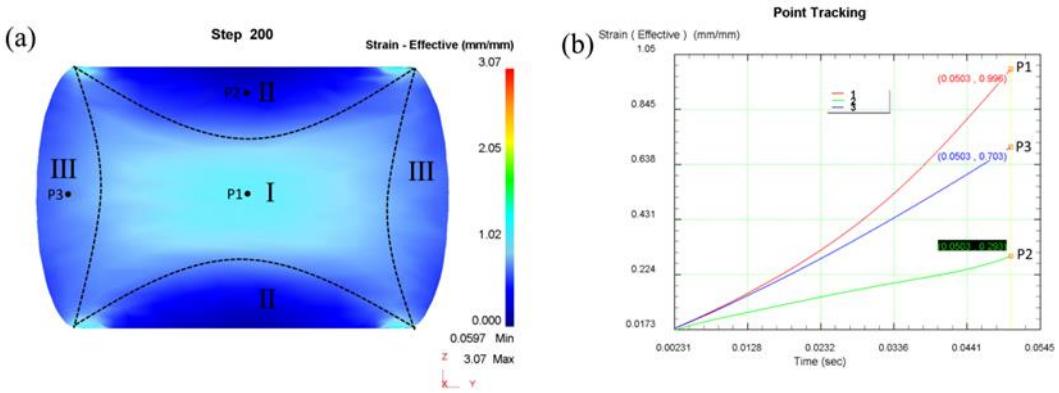

Fig. 7. (a) Effective strain distribution at different regions, (b) the effective strain-time curves of the Point 1, Point 2 and Point 3.

The strain distributions of deformed specimen have a major impact on the material's microstructure. Therefore, it's necessary to study deformed specimen's internal strain distribution. The effective strain distribution on the deformed specimen's axial section is shown by Fig. It shows that the effective strain is unevenly distributed. According to the effective strain distribution, the axial section is divided into three regions [10]: (1) Domain I, which was called the large deformation region with relatively large level of deformation at the center of specimen; (2) Domain II, which was the bonded region at both ends of the deformed specimen, this region has relatively small deformation due to friction between the workpiece and the die; (3) Domain III was called free deformation region, which is located at the edge of the deformed specimen. The deformation level in domain III is higher than that in domain II, but lower than that in domain I. To further study the changes of effective strain under different regions during the hot deformation process, Point 1, Point 2 and Point 3 were selected as the feature points in domain I, domain II and domain III. Fig. 7 (b) is the effective strain vs. time curves of the selected points. It indicated that the effective strain at point 1 increases rapidly with time, and the maximum effective t strain is 0.996. The effective strain at point 2 increases slowly with time, and the maximum effective strain is only 0.293. The effective strain at point 3 during deformation is higher than that at point 2 but lower than that at point 1, and the maximum value of the effective strain is 0.703. Fig. 8 shown the simulation results of stress-time curve at varying deformation conditions. It indicates the effective stress increases rapidly with time in initial stage. When the peak stress is reached, the effective stress gradually stabilizes with time. The variation trend of flow stress is consistent with the test data. To further verify the accuracy of simulation results. According to Eq. 13, the simulated stress-time curves can be converted into the stress-strain curves, and compared with the experimentally obtained flow curves. The comparison between experimental results and stress-strain curve simulation results at varying deformation conditions are shown in Fig. 9. The results indicate that the finite element analysis results are consistent with the corresponding test results.

$$\varepsilon = -\ln(1 - \dot{\varepsilon}t) \tag{13}$$

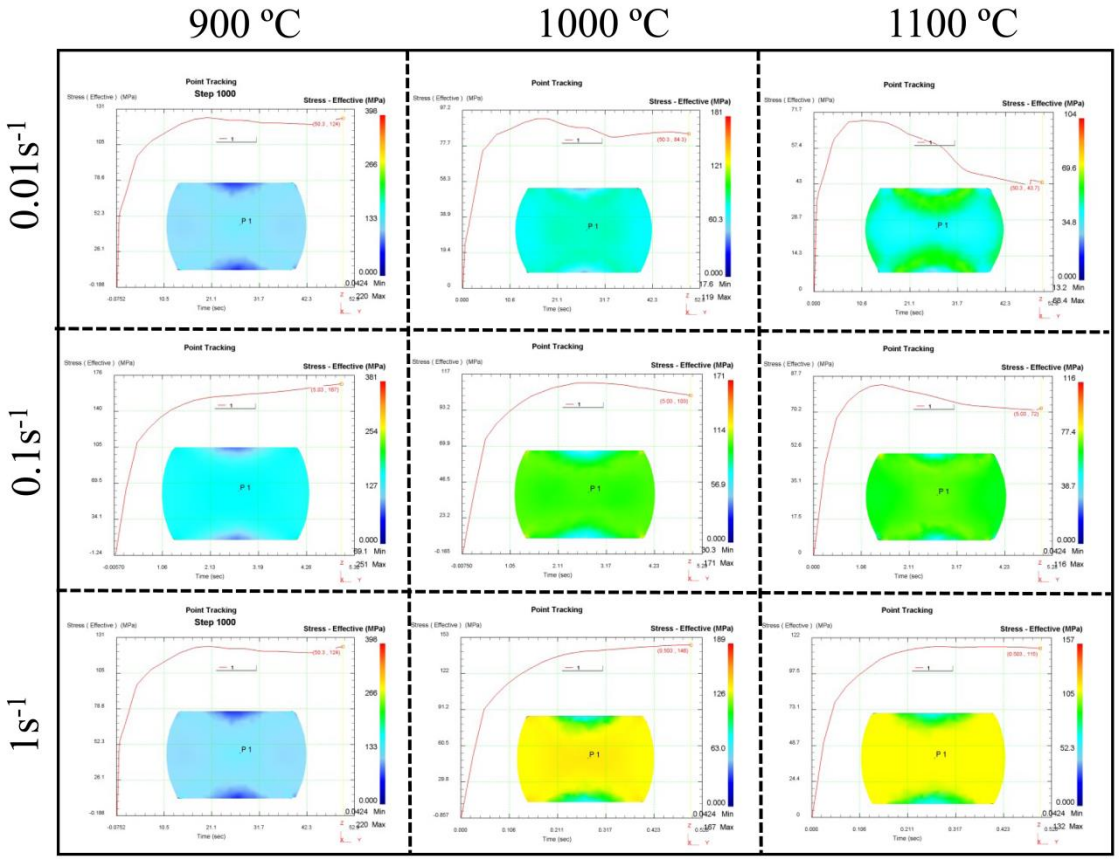

Fig. 8. The simulation results of the stress-time curves at varying strain rates and deformation temperatures.

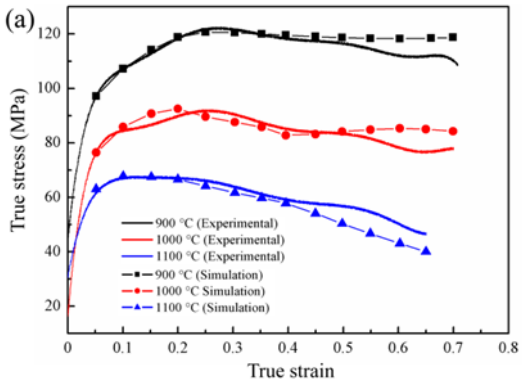

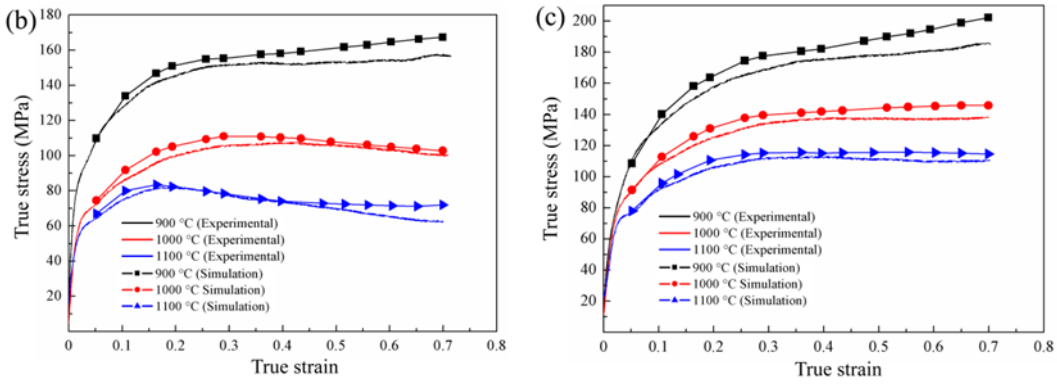

Fig. 9. Comparison between the simulation and experimental true stress-strain curves at different temperatures and strain rates: (a) 0.01 s^{-1}, (b) 0.1 s^{-1}, (c) 1 s^{-1}.

4. Conclusions

In this paper, the flow behavior of HSLA steel during isothermal compression at different deformation conditions was investigated, the flow stress increases as the strain rate increases or the deformation temperature decreases. The peak stress constitutive equation was established and the apparent activation energy be calculated as 437955 J/mol. The effective strain distribution and flow stress of HSLA steel during isothermal compression were investigated by using FEA method, and the stress-strain curves obtained by FEM are consistent with the corresponding test results.

Acknowledgements

This paper is funded by the International Exchange Program of Harbin Engineering University for Innovation-oriented Talents Cultivation.

References

[1] X. Chen, Y. Huang, J. Alloy. Compd. 619 (2015) 564-571.
[2] R. Shukla, S.K. Das, B.R. Kumar, S.K. Ghosh, S. Kundu, S. Chatterjee, Metall. Mater. Trans. A-Phys. Metall. Mater. Sci. 43A (2012) 4835-4845.
[3] A. Galibois, M.R. Krishnadev, A. Dubé, Metall. Trans. A 10 (1979) 985-995.
[4] A. Momeni, H. Arabi, A. Rezaei, H. Badri, S.M. Abbasi, Mater. Sci. Eng. A 528 (2011) 2158-2163.
[5] M. Klein, H. Spindler, A. Luger, R. Rauch, P. Stiaszny, M. Eigelsberger, Mater. Sci. Forum. 500-501 (2005) 543-550.
[6] H.L. Wei, G.Q. Liu, X. Xiao, H.T. Zhao, H. Ding, R.M. Kang, Mater. Sci. Eng. A 564 (2013) 140-146.
[7] M.R. Rahul, S. Samal, S. Venugopal, G. Phanikumar, J. Alloy. Compd. 749 (2018) 1115-1127.
[8] L. Zhou, C. Cui, Q.Z. Wang, C. Li, B.L. Xiao, Z.Y. Ma, J. Mater. Sci. Technol. 34 (2018) 1730-1738.
[9] Z.J. Wang, L.H. Qi, G. Wang, H.J. Li, M.S. Dargusch, Mech. Mater. 102 (2016) 90-96.
[10] Y. Xu, C. Chen, X.X. Zhang, H.H. Dai, J.B. Jia, Z.H. Bai, Mater. Charact. 145 (2018) 39-52.